Accuracy of real time noninvasive temperature measurements using magnetic resonance thermal imaging in patients treated for high grade extremity soft tissue sarcomas

Oana I. Craciunescu[a] and Paul R. Stauffer
Department of Radiation Oncology, Duke University Medical Center, Durham, North Carolina 27710

Brian J. Soher
Department of Radiology, Duke University Medical Center, Durham, North Carolina 27710

Cory R. Wyatt
Department of Biomedical Engineering, Duke University Medical Center, Durham, North Carolina 27710

Omar Arabe, Paolo Maccarini, Shiva K. Das, and Kung-Shan Cheng
Department of Radiation Oncology, Duke University Medical Center, Durham, North Carolina 27710

Terence Z. Wong
Department of Radiology, Duke University Medical Center, Durham, North Carolina 27710

Ellen L. Jones, Mark W. Dewhirst, and Zeljko Vujaskovic
Department of Radiation Oncology, Duke University Medical Center, Durham, North Carolina 27710

James R. MacFall
Department of Radiology, Duke University Medical Center, Durham, North Carolina 27710 and
Department of Biomedical Engineering, Duke University Medical Center, Durham, North Carolina 27710

(Received 26 April 2009; revised 7 August 2009; accepted for publication 21 August 2009; published 2 October 2009)

Purpose: To establish accuracy of real time noninvasive temperature measurements using magnetic resonance thermal imaging in patients treated for high grade extremity soft tissue sarcomas.
Methods: Protocol patients with advanced extremity sarcomas were treated with external beam radiation therapy and hyperthermia. Invasive temperature measures were compared to noninvasive magnetic resonance thermal imaging (MRTI) at 1.5 T performed during hyperthermia. Volumetric temperature rise images were obtained using the proton resonance frequency shift (PRFS) technique during heating in a 140 MHz miniannular phased array applicator. MRTI temperature changes were compared to invasive measurements of temperature with a multisensor fiber optic probe inside a #15 g catheter in the tumor. Since the PRFS technique is sensitive to drifts in the primary imaging magnetic field, temperature change distributions were corrected automatically during treatment using temperature-stable reference materials to characterize field changes in 3D. The authors analyzed MRT images and compared, in evaluable treatments, MR-derived temperatures to invasive temperatures measured in extremity sarcomas. Small regions of interest (ROIs) were specified near each invasive sensor identified on MR images. Temperature changes in the interstitial sensors were compared to the corresponding ROI PRFS-based temperature changes over the entire treatment and over the steady-state period. Nonevaluable treatments (motion/imaging artifacts, noncorrectable drifts) were not included in the analysis.
Results: The mean difference between MRTI and interstitial probe measurements was 0.91 °C for the entire heating time and 0.85 °C for the time at steady state. These values were obtained from both tumor and normal tissue ROIs. When the analysis is done on just the tumor ROIs, the mean difference for the whole power on time was 0.74 °C and during the period of steady state was 0.62 °C.
Conclusions: The data show that for evaluable treatments, excellent correlation ($\Delta T < 1$ °C) of MRTI-ROI and invasive measurements can be achieved, but that motion and other artifacts are still serious challenges that must be overcome in future work. © *2009 American Association of Physicists in Medicine*. [DOI: 10.1118/1.3227506]

Key words: noninvasive temperature measurement, soft tissue sarcoma, proton resonance frequency shift method

I. INTRODUCTION

Soft tissue sarcomas (STS) comprise of approximately 1% of all malignant tumors. In the United States, the incidence of STS is approximately 9000 new cases per year. The histology and presentation are quite heterogeneous. The overall 5 yr survival remains approximately 50%–60% for all stages and sites combined.[1] Multidisciplinary management is essen-

tial for optimal treatment. Novel approaches incorporating chemotherapy agents with more intensive dose schedules may improve response rates and survival.

For extremity STS, local control rates of 70%–90% have been reported with combinations of radiation and surgery including preoperative or postoperative external beam radiation therapy[2] or brachytherapy in the immediate postoperative setting.[3] At Duke University Medical Center, local control of 94% has been achieved with preoperative regional hyperthermia (HT) combined with concurrent external beam radiation, but with an approximate 50% frequency of distant metastases.[4] More recently, Issels *et al.*[5] reported on the results of the European Organization for Research and Treatment of Cancer (EORTC) Phase III trial on neoadjuvant chemotherapy alone versus chemotherapy in conjunction with regional hyperthermia for patients with locally advanced high grade STS. They showed that regional hyperthermia improves response and survival when combined with systemic chemotherapy vs. chemotherapy alone.

The efficacy of hyperthermia for cancer therapy is dependent on the delivery of well-controlled moderate heating (41–45 °C) to the entire tumor volumes without overheating the surrounding critical normal tissues. Traditionally, per international guidelines,[6–9] monitoring of hyperthermia treatments is done with invasive temperature probes. However, such a thermometry system has many disadvantages: Low acceptance in patients, time-consuming invasive placement with risk of hemorrhage, infection, low density of temperature samples, and potentially increased risk of metastasis. Moreover, invasive thermometry lacks the ability to provide volumetric information that is needed to control power delivery from newer more adjustable heating systems and to provide adequate thermal dosimetry for subsequent correlation with clinical response. To address this issue, at least two strategies have been identified:[10] Recording temperatures at a limited number of "tumor-related reference points," which are reachable intraluminally (rectum, vagina, bladder, and urethra), and the use of noninvasive MR thermometry for 3D dosimetry that has significant potential to automate and improve the quality of HT treatments.

Noninvasive MR thermometry has been investigated for more than a decade to assist in the delivery of the HT treatments and can offer better characterization of the treatment efficacy by allowing the calculation of the required thermal metrics from the volumetric data. Moreover, MR imaging offers opportunities for validation of treatment planning systems,[11,12] dynamic control of treatment delivery,[13–15] and post-treatment assessment of tissue damage.[16] Magnetic resonance thermal imaging (MRTI) has been developed and applied mainly to assist in delivering thermal therapies like laser, radiofrequency, and high intensity focused ultrasound.[17] The International Journal of Hyperthermia summarized in a special issue the current status of MR thermometry.[18–21] Additional background can be found in the review article of Rieke and Pauly[22] and in the RSNA Refresher Course "MR imaging in hyperthermia."[23]

The use of noninvasive MR thermometry in STS has been described in phantoms and human patients at Duke University,[24–26] at Klinikum Grosshadern (Munich, Germany),[27] and most recently and comprehensively at the University Hospital Charite (Berlin, Germany).[28] The Charite group performed a detailed study to evaluate noninvasive MR thermometry for monitoring HT treatments in patients with STS of the lower extremities and pelvis. They found an excellent correlation between pathohistologic response and CEM43T90 (cumulative equivalent minutes at 43 °C to 90% of the target volume) and also an excellent correlation between the invasive and the noninvasive MR temperatures (R^2=0.96). The treatments were done in a hybrid system that integrates a multiantenna applicator, Sigma Eye (BSD 2000/3D, BSD Corporation, Salt Lake City, UT) into a 1.5 T MR scanner (Siemens Magnetom Symphony, Erlagen, Germany). They have previously addressed the feasibility of performing noninvasive MR thermometry in this hybrid system[12] and more recently the issue of imaging artifacts.[29]

The current system at Duke University for performing HT treatments of extremity STS patients aided by MRTI is a dedicated 1.5 T GE scanner (Signa Excite, GE Healthcare, Milwaukee, WI) together with a miniannular phased array (MAPA) applicator operated at 140 MHz. This GE Excite scanner/MAPA applicator combination was not characterized previously with respect to the acuity of MR noninvasive temperature measurements. The purpose of this study is to characterize the accuracy of temperatures measured noninvasively with MRTI when compared to the existing gold standard of invasive thermometry with fiber optic probes in patients with high grade STS as established with the scanner/applicator combination in use currently at our institution.

II. MATERIALS AND METHODS

II.A. Clinical protocol

Selected patients with high grade extremity STS, i.e., patients that could be heated in the MAPA applicator, were treated at our institution on an IRB approved protocol using standard radiotherapy and hyperthermia with or without chemotherapy. The treatment consisted of 45 Gy over 25 fractions and once a week HT for 5 weeks, followed by surgical resection after 3–5 weeks in a setting that allows the use of a 1.5 T MR scanner for noninvasive MRTI. MR perfusion imaging studies were performed on heated patients before the start of treatment (baseline) and 24 h after the first HT treatment using dynamic contrast-enhanced magnetic resonance imaging (DCE-MRI).

The primary goal of this clinical investigation was to determine the feasibility and accuracy of real time noninvasive magnetic resonance image based thermometry in the monitoring and control of hyperthermia treatments of extremity STS. A secondary goal of the study, not presented here, was to determine if measurements of tumor physiology as defined by DCE-MRI studies are predictive of clinical and/or pathologic response, and/or metastatic potential.

Initially, the protocol was written for the first HT treatment to be delivered with conventional thermometry and

only subsequent treatments with the integrated MAPA/MR system. Heatability was to be determined after the first HT treatment by the following criteria: (1) The tumor must be located on an extremity and must anatomically fit within the radiofrequency array heating device and (2) the patient must achieve a CEM 43T90 of at least 0.5 min for the first treatment. If a patient was unheatable, then therapy proceeded as outlined in the protocol except hyperthermia was omitted. Starting with the fifth patient, we completed all HT treatments in the MR suite, given its availability.

II.B. Ancillary studies: DCE-MRI

The day before the first HT treatment, the patients underwent a DCE-MRI scan performed on the same 1.5 T GE scanner used for MRTI using a 60 cm diameter body coil. After an axial three-plane, 2D localizer, several 3D T1-weighted fat-suppressed gradient-recalled echo sequence with TR/TE, 5.4/1.4 ms, flip angle $=5°, 10°, 15°, 20°, 30°, 45°, 60°$, FOV$=24$ cm^2, 256×256 matrix, and variable slice thickness between 8 and 10 mm were acquired. The different flip angle scans were acquired to generate T_{10} (noncontrast-enhanced tissue relaxation time) maps needed for the pharmacokinetic analysis.[30] After five baseline scans at 30° flip angle, gadopentetate dimeglumine (Magnevist [0.1 mmol/kg of body weight], Berlex, Wayne, NJ) was administered by a rapid injector through an indwelling IV catheter at a rate of 2 cm^3/s. Contrast-enhanced imaging was initiated immediately after the contrast agent was completely injected and consisted of two volume acquisitions through the area of interest: One was performed over 10–12 min in rapid succession (i.e., no delays) immediately after contrast administration and the second was performed after a 3 min delay from the end of the first acquisition. All contrast-enhanced imaging was performed with the same T1-weighted sequence optimized before contrast injection with a flip angle of 30°. Unenhanced and contrast-enhanced MRI examinations were performed in axial cuts, with a temporal resolution of 30–40 s per volume and an approximate total imaging time of 15–20 min per examination. The number of slices varied depending on size of the imaged volume.

Subtraction images were generated between the maximum enhancement scan (approximately at time 60–80 s after injection) and the baseline scan to help define highly perfused and necrotic areas of the tumor for HT catheter placement.

II.C. MRTI monitored hyperthermia treatment

The protocol calls for placement of at least one interstitial catheter centrally across the tumor mass allowing insertion of four 0.56 mm diameter fiber optic sensors (model 3100 sensors, Luxtron Corp., Santa Clara, CA). The catheter was placed aided by DCE-MRI images acquired usually the day before the first HT treatment and verified with a MR localizer. These DCE-MRI images gave additional information about the perfusion status of a tumor helping to direct the probe to monitor at least three types of physiologically diverse tissue: Normal tissue, viable tumor, and necrotic tumor (if any). Based on the length of the catheter insertion, the fiber optic probes are staggered 1–2 cm apart in the catheter. Generally, the catheter was oriented oblique to the scan planes such that the four fiber optic sensors were located in four different image planes. Further MR localization was necessary to depict the four slices that were imaged with MRTI. The slices were defined to be centered with the known location of the fiber optic probe for further comparison between MR thermometry and invasive thermometry.

The HT treatments were performed using a cylindrical RF phased array applicator (MAPA) (inner diameter=23 cm, outer diameter=25 cm, and length=30 cm) that contains four pairs of flared dipoles positioned symmetrically around the circumference of the cylinder.[31] The four twin-dipole antennas are driven with independent phase and amplitude signals at 140 MHz, allowing the generation of a phase focus at the center of the array that can be shifted laterally by adjustment of the relative phase of the four dipoles. This applicator was intended for heating tumors located anywhere in an extremity that can fit anatomically inside the cylinder while allowing space for the water bolus that provides dielectric coupling between the antennas and the patient. In the initial design, four external water-filled references were incorporated. A modified version of the MAPA was used later in the trial, which incorporates internal (inside the applicator) silicone oil filled tubes that allow for drift correction (see Secs. II D and III).

II.D. Magnetic resonance thermal imaging (MRTI)

With the patient in treatment position, the MRTI monitored HT treatment commenced. The technique used by our group is based on the dependence of the proton resonance frequency shift (PRFS) of water with temperature.[23,32,33] The PRFS method has been shown to provide the best temperature sensitivity and is now the most commonly used approach for monitoring tissue temperature rise with MR. It's successful use in aiding HT or thermal ablative procedures has been documented and summarized recently by Rieke and Pauly[22] and by MacFall and Soher.[23]

A major difficulty with PRFS-based imaging is that of image phase "drift" over the time of a series of temperature measurements during a typical HT treatment (1–1.5 h). Depending on the scanner, the image phase may drift enough to make the PRFS method unusable. During this protocol, the heating applicator design was modified to include four 1 cm diameter cylindrical temperature-stable silicone oil references inside the MAPA water bolus to allow for drift correction. The phase changes in the oil references were fit to the entire image using a minimum curvature spline surface fitting algorithm,[34] which provides a first order fit when using four references. Although generally not necessary, a second order fit can be achieved with more references, improving the correction of the drift in some cases.[35] The efficacy of the correction was investigated in phantoms[23,35] and applied in the last three patients on the protocol. Other investigators have solved field gradient drift problems in a similar manner,

inserting temperature-stable references in the image plane and correcting all pixels of the image to cancel any apparent temperature change in the references.[11,19]

Prior to application of RF power, the PRFS sequence acquisition started with a set of four sequential MR slices acquired at 1 min interval to establish baseline temperature conditions. The imaging was done using the 60 cm body radiofrequency coil of the 1.5 T GE Signa Excite scanner. The parameters for the 2D axial RF spoiled gradient sequence were TR/TE 34.5/20 ms, flip angle=30°, FOV =30 cm^2, 256×256 matrix, N_{ex}=4, BW=15.6 kHz, and slice thickness of 20 mm, no gap. N_{ex}=4 was used to obtain a good signal-to-noise ratio (typically 115 in a tumor and 90 in muscle).

For this study, a custom image analysis platform was developed at Duke University that allows real time acquisition of PRFS images in multiple MR slices with software capability to delineate user defined regions of interest (ROIs) in which average tissue temperature rise above baseline is calculated. Initially, i.e., for the first seven patients, four small ROIs were defined inside the external reference tubes for drift correction. If only external references were available, the data were used for analysis only if either no drift was recorded for that treatment, or if the drift was correctable with the external references, i.e., external references did not change temperature with heating. For the patients heated in the modified MAPA that included internal references, the small ROIs used for drift correction were defined in the internal silicon-filled references. The temperature analysis program was initiated with these reference values to correct for drifts in the magnetic field gradient magnets during the ensuing HT treatment.

During the HT treatment, ROIs are specified in each MR slice in user determined regions of interest such as center and periphery of tumor, entire tumor, and critical normal tissue regions in which to avoid heating, etc. The graphical user interface provides real time continuous display of temperature rise vs treatment time for all selected ROIs overlaid on the data from the four Luxtron fiber optic sensors.

II.E. Invasive temperature vs MR temperature validation study

For the retrospective correlation study between MR and invasive thermometry, a ROI was drawn on each slice in the close vicinity to the fiber optic temperature sensor in that plane. The ROIs varied in size from 36 to 58 pixels, with the pixel size of approximately 1 mm. If the fiber optic location on a given plane was not known with certainty, data from that slice were not used for the correlation study. The PRFS method was used to calculate temperature rise of each voxel in four MR image planes, normally taken at 1.5–2 cm intervals through the tumor. Four 2D temperature rise images were reconstructed from this dataset once per minute, each referenced back to the initial baseline images taken prior to initiating heat treatment.

For exemplification, three representative ROIs were selected, one in viable tumor, one in necrotic tumor, and one in normal tissue, at the tumor/fat interface. A qualitative comparison was performed by superimposing the two temperature curves. For a quantitative comparison, a Bland–Altman analysis was used.[36] Bland–Altman plots are useful to compare a new measurement technique or method with a gold standard. Each of the samples is represented on the graph by assigning the mean (average) of the two measurements as the abscissa (x axis) value, and the difference between the two values as the ordinate (y axis) value. Horizontal lines are drawn at the mean difference, and at the mean difference plus and minus 1.96 times the standard deviation of the differences. To further visualize the correlation between the two methods for temperature measurement, scatterplots with regression lines were generated for each of the three ROIs, and the regression coefficients were calculated.

For the overall comparison, the ROI size in pixels, time, and the corresponding mean and standard deviation of the MR calculated change in temperature were recorded for each ROI and compared to the change in temperature given by the invasive thermometry sensor by defining an absolute difference between the two.

For each ROI, the mean and standard deviation were calculated for the whole power on time and also for part of the treatment for which steady state was achieved. If no apparent steady state was reached, then the value from 20 min after power on until end of the treatment was used. To determine the overall correlation between MR and invasive temperature measurements, the mean absolute difference is reported for all ROI for the whole treatment and for the period of steady state, as well as the mean absolute difference for tumor ROIs and normal ROIs separately.

III. RESULTS

III.A. Clinical protocol

Since 2004, 15 patients with grade 2 or 3 soft tissue sarcomas of the extremities were enrolled on the study, of which 10 were heated, for a total of 50 HT treatments. Reasons for taking a patient off protocol included noncompliance (1), nonheatable per initial protocol criteria (1), tumor too large for applicator (2), and pulmonary embolism (1). The heated tumors were located as follows: 2 thigh, 4 calf, 2 forearm, 1 wrist, and 1 upper arm. Of the 50 HT treatments, 10 were treated outside the magnet, 5 first fractions per initial protocol to establish heatability, and the remaining due to scanner down time, and thus not included in the analysis.

III.B. MRTI monitored hyperthermia treatment

Catheters were inserted for invasive thermometry at each HT treatment. The subtraction images generated from the DCE-MRI scan acquired the day before the first HT treatment were used to initially guide the catheter placement. Figure 1(a) shows a DCE-MRI subtraction image between the baseline and the maximum intensity scan (60 s postcontrast agent injection) used to guide the catheter placement to acquire data from three physiologically diverse areas: Normal tissue, viable tumor, and necrotic area (if any). Figure

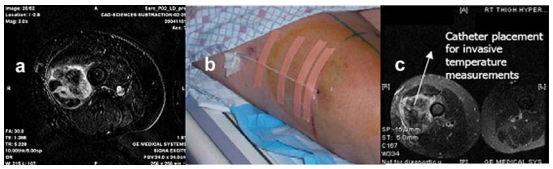

FIG. 1. (a) DCE-MRI subtraction image between the baseline and the maximum intensity scan (60 s postcontrast agent injection) used to guide the catheter placement to acquire data from three physiologically diverse areas: Normal tissue, viable tumor, and necrotic tumor (if any). (b) Image showing catheter placement in one of the patients with a right thigh high grade STS. (c) Postcatheter insertion MR verification, showing the catheter spanning the three areas to be monitored: Normal tissue, viable tumor, and necrotic core.

1(b) shows an image of a catheter placement in one of the patients with a RT thigh high grade STS. A postcatheter insertion MR verification is shown in Fig. 1(c), depicting the catheter spanning the three areas to be monitored: Normal tissue, viable tumor, and necrotic core.

The MR localization scans performed in the early patients had variable success in identifying exact locations of the catheter relative to tumor as the air filled catheter did not contrast well against many tissues. An adjustment to the scan procedure in later patients provided significantly improved visualization of the catheter by inserting a smaller diameter catheter filled with gadolinium for the preocalization scan. This facilitated precise localization of the catheter in the tumor and subsequent calculation of the position of the four staggered Luxtron sensing points.

From the first ten patients that underwent HT treatments under this protocol, seven were treated using the original MAPA design and three treated with the drift compensation-ready MAPA.

Examples of patients with extremity STS are shown in Figs. 2(a)–2(c), showing the tumor bearing extremity inserted into the cylindrical MAPA applicator with the tumor centered within the four twin-dipole antennas. For the first cohort of patients, the bolus was filled completely around the extremity with de-ionized water at 42 °C. The patient was then moved into the MR magnet, RF power cables attached, and input impedance parameters measured for the four antennas. Figure 2(c) shows the integration of the patient and MAPA applicator into a 1.5 T GE scanner for temperature monitoring using MRTI.

Following the initial baseline scans, approximately 20–50 W of power at 140 MHz was applied to each of the four

FIG. 2. (a) MAPA positioning for a patient with a lower extremity STS. Tape shown on patient's leg holds a single invasive #15 g catheter in place which extends diagonally across the tumor volume and is filled with four stationary Luxtron 3100 fiber optic sensors spaced 1.5 cm apart along the catheter [seen better in Fig. 1(b)];. (b) MAPA positioning for a patient with upper extremity STS. (c) Patient inside MAPA and 1.5 T MR scanner ready for treatment.

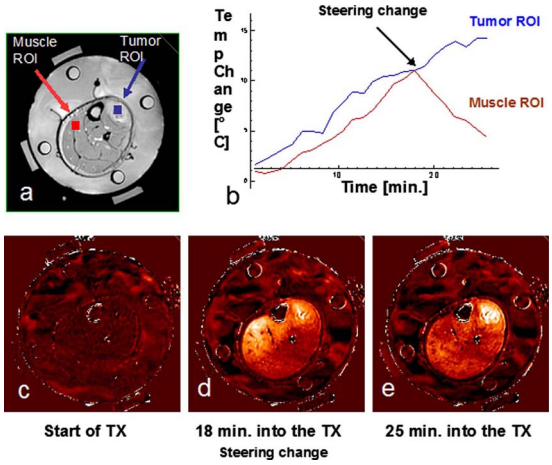

FIG. 3. Summary of HT treatment: (a) Axial MRI image of the patient's lower extremity inside the MAPA applicator as seen in Fig. 2(a). (b) Temperature data as a function of time for two regions of interest: Muscle (normal tissue) ROI and tumor ROI. (c) Baseline temperature change map after 4 min of imaging without application of heat, temperatures in the leg are stable at about 36 °C. (d) Temperature rise image at approximately 18 min into treatment heating of tumor is visible but is less than undesirable heating of normal tissue on the upper left side of leg. (e) 25 min into treatment, after adjusting the antenna phases, heat is focused primarily in the tumor region creating a large differential heating of tumor.

antennas, initially with equal phases and amplitudes to produce a central zone of heating deep in the extremity. As the tissue is heated, the MR imaging of four slices through the tumor continued at 1 min interval. A drift correction mechanism was implemented in our MRTI treatment console. An example of a treatment where images were corrected using this method is shown elsewhere.[23]

The potential of using the real time MRTI data to guide the treatment is demonstrated in Fig. 3. During treatment, the tumor temperature as recorded by both the invasive probe, and tumor ROI was rising but the MR image showed significant temperature rise in the normal muscle tissue as well. At 18 min into the treatment, the relative phases of the four antennas were adjusted to refocus heating away from the normal tissue and into the tumor. The net effect of these phase adjustments is seen by rising temperatures in the invasive tumor sensors as well as enhanced differential temperature change in the tumor vs normal tissue ROIs on the MRTI image. Figure 3 shows the initial baseline image (c), followed by a diffuse heating pattern developing after 18 min of central focus with 0,0,0,0 phases (d), and finally the effective shifting of heat focus into the tumor by 25 min into treatment due to the change in relative antenna phases to 0,30,60,30.[37] The steering of power is possible in our setting as the image transfer from the MR console to the analysis software is fast (within a minute of acquisition). A few other minutes are needed to analyze the images and determine the need for steering. Once a sufficient number of scans have been acquired to decide the need for steering, changes in phase and amplitude can be implemented and the results displayed within a few minutes, giving the whole procedure a real time characteristic.

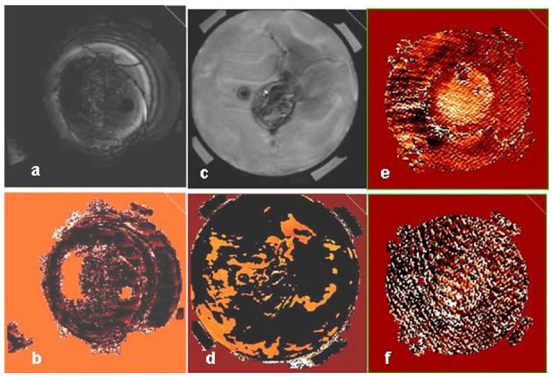

FIG. 4. Examples of intrascan motion artifacts that disqualified a certain treatment or time point from the validation analysis: Magnitude image for a lower (a), upper (c) extremity patient. [(b) and (d)] Change in phase images for same patients as in (a) and (c). [(e) and (f)] change in phase images showing artifacts at two distinct time points during the treatment. In such cases, only those specific time points were discarded.

III.C. Invasive temperature vs MR temperature validation study

We analyzed MRTI images and compared to invasive temperatures measured in extremity sarcomas over 40 heat treatments. The validation study was performed with data from 6/10 heated patients. Studies were discarded from this analysis due to lack of MR information in HT treatments performed outside the MR scanner, image/motion artifacts, uncorrectable drift, impossibility to localize with certainty the Luxtron fiber optic probes, and missing (corrupted) Luxtron data files. The motion artifacts encountered were either intrascan motion (motion during MR acquisition) resulting in visible blurring or ghosting artifacts, or interscan motion that occurred as a result of patient movement between subsequent MR acquisitions. The latter was detected when movies of each slice were played from power on to power off. Examples of MR treatments discarded due to intrascan artifacts are shown in Fig. 4.

Three representative ROIs were selected for a more detailed analysis: A viable tumor ROI (from patient P14, posterior calf tumor), necrotic tumor (from patient P08, right upper forearm tumor), and an ROI at the tumor/fat interface (from patient P13, left anterior leg tumor).

Figures 5–7 show comparisons between Luxtron fiber optic probe measurements and MR measurements in the viable (v) tumor ROI (Fig. 5), the necrotic (n) tumor ROI (Fig. 6), and the tumor/fat interface ROI (Fig. 7). In each of the three figures, panel (a) represents an axial MR image with superimposed ROI, panel (b) shows the change in temperature (delta*T*), in °C (degC) over the time of the treatment as measured in the specified ROI with Luxtron invasive dosimeters (Delta*T*_LUX), and MR thermometry (Delta*T*_MR), and panel (c) shows a Bland–Altman plot comparing the MRTI

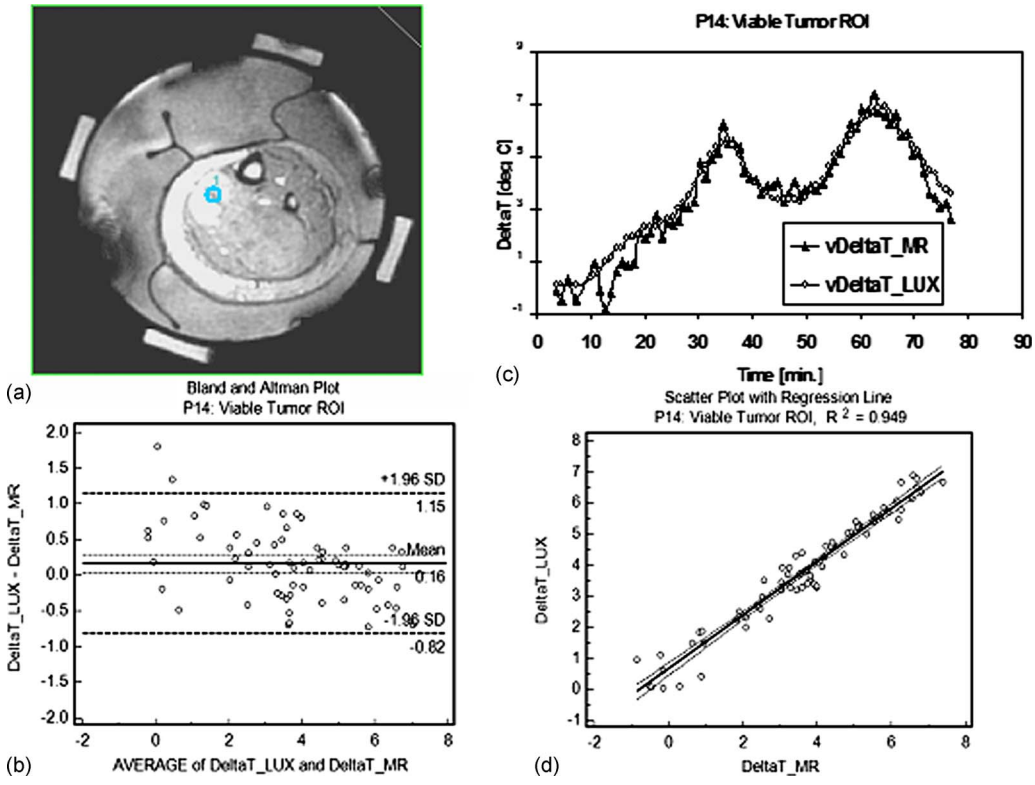

FIG. 5. Comparison between Luxtron fiber optic probe measurements and MR measurements in a viable (v) Tumor ROI: (a) MR image with a 56 pixel ROI superimposed. (b) Change in temperature (delta*T*), in °C (degC) over the time of the treatment as measured in the specified ROI with Luxtron invasive dosimeters (vDelta*T*_LUX) and MR thermometry (vDelta*T*_MR) with continuous power application between 80 and 200 W. (c) Bland–Altman plot comparing the MRTI temperatures with Luxtron temperatures. The mean and 95% limit of agreement are indicated on the graph (values in Table I). (d) Scatterplot with regression line indicated between the Luxtron measurements and the MR measurements: R^2=0.949.

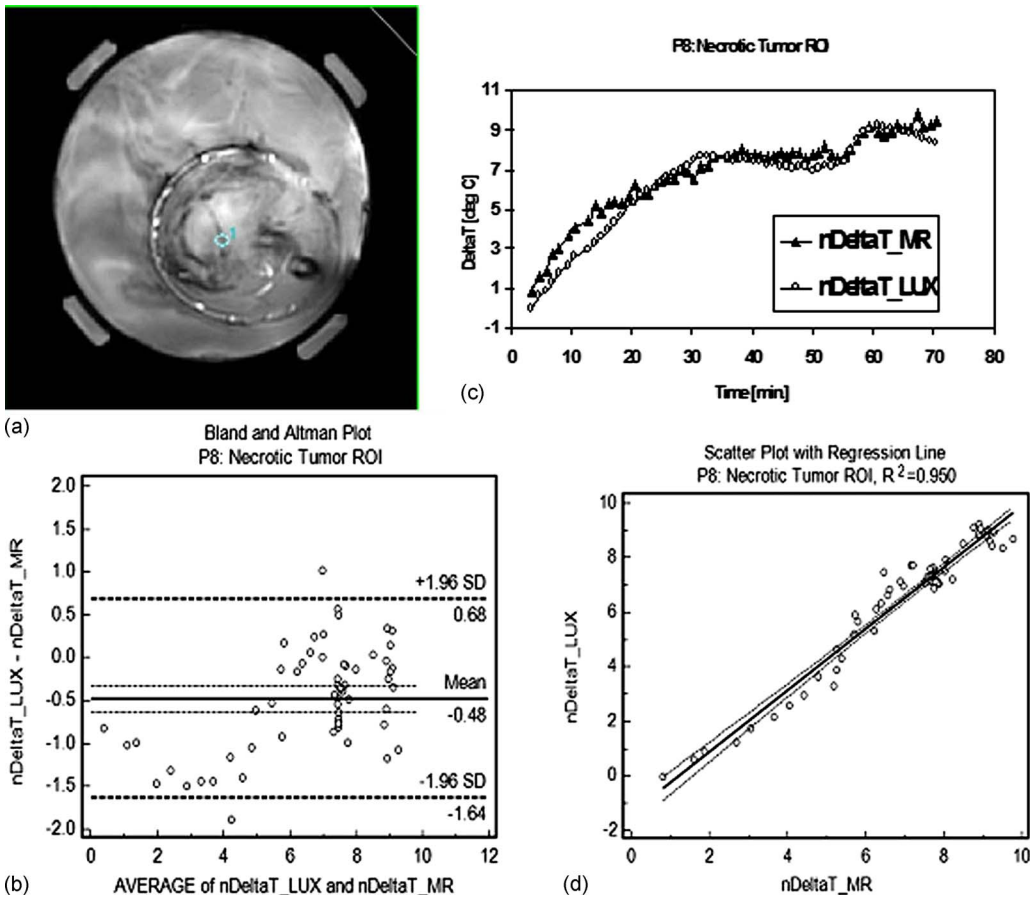

FIG. 6. Comparison between Luxtron fiber optic probe measurements and MR measurements in a necrotic (n) Tumor ROI: (a) MR image with a 52 pixel ROI superimposed. (b) Change in temperature (delta$T$), in °C (degC) over the time of the treatment as measured in the specified ROI with Luxtron invasive dosimeters (nDelta$T$_LUX) and MR thermometry (nDelta$T$_MR) with continuous power application between 100 and 160 W. (c) Bland–Altman plot comparing the MRTI temperatures with Luxtron temperatures. The mean and 95% limit of agreement are indicated on the graph (values in Table I). (d) Scatterplot with regression line indicated between the Luxtron measurements and the MR measurements: $R^2=0.950$.

temperatures to Luxtron temperatures. The mean and 95% limit of agreement are indicated on the graphs, and the values are summarized in Table I. Subplot (d) in each of Figs. 5–7 represent scatterplots between the Luxtron measurements and MR measurements with regression lines indicated: $R^2=0.949$ for the viable tumor ROI, $R^2=0.950$ for the necrotic tumor ROI, and $R^2=0.740$ for the tumor/fat interface ROI.

Table I summarizes the results for the three ROIs considered: Viable tumor, necrotic tumor, and tumor/fat interface (considered as normal tissue) based on a Bland–Altman comparison between Luxtron and MR measurements. The results included are the mean of differences ±95% CI, the standard deviation, and the lower and upper limit ±95% CI.

With data collected from 28 ROIs from the 6/10 extremity sarcoma patients that underwent HT treatments in the MR, the mean difference between the MRTI measured temperatures and the interstitial point measurements during the whole power on time was 0.91 °C and during the period of steady state was 0.85 °C. These values were obtained from both tumor and normal tissue ROIs. When the analysis is done on just the tumor ROIs, the mean difference for the whole power on time was 0.74 °C and during the period of steady state was 0.62 °C. The invasive thermometry available to sample normal tissue was limited and usually included measurements in regions at muscle/fat or tumor/fat interfaces, making the MR temperature data more noisy and prone to volume averaging effects across the interface. For this reason, the mean difference between the invasive Luxtron fiber optic probes and MR thermometry was 1.89 °C for the whole treatment and 2.12 °C for steady state in these few normal tissue comparison points (13% of all analyzed ROIs). The poorer agreement is visible in Fig. 7.

IV. DISCUSSION

A critical need has emerged for volumetric thermometry to visualize 3D temperature distributions in real time during deep hyperthermia treatments used as an adjuvant to radiation or chemotherapy for cancer. Previous use of the RF phased array applicator monitored only by invasive fiber optic thermometry did not have a sufficient number of thermal monitoring points to allow proper visualization of the 3D heating pattern necessary for effective steering of heating

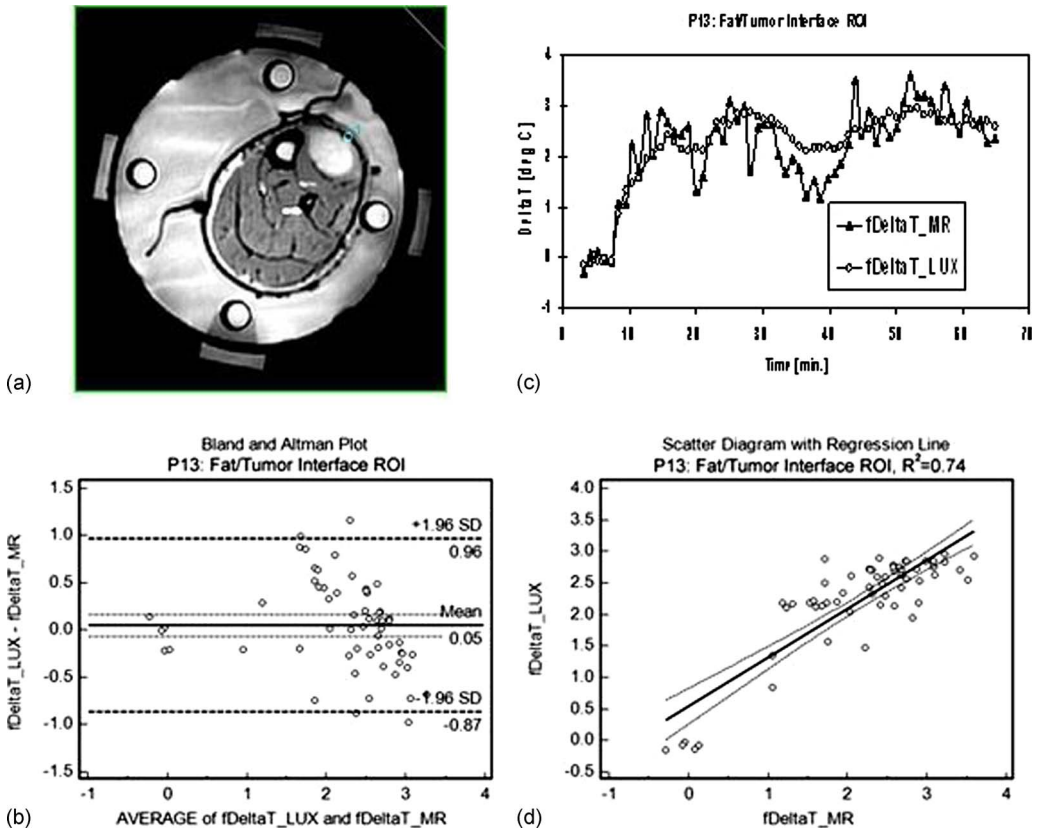

FIG. 7. Comparison between Luxtron fiber optic probe measurements and MR measurements in a fat/tumor interface (f) ROI: (a) MR image with a 32 pixel ROI superimposed. b) Change in temperature (delta*T*), in °C (degC) over the time of the treatment as measured in the specified ROI with Luxtron invasive dosimeters (fDelta*T*_LUX) and MR thermometry (fDelta*T*_MR) with continuous power application between 40 and 80 W. (c) Bland–Altman plot comparing the MRTI temperatures with Luxtron temperatures. The mean and 95% limit of agreement are indicated on the graph (values in Table I). (d) Scatterplot with regression line indicated between the Luxtron measurements and the MR measurements: $R^2=0.740$.

focus into the tumor. This often left parts of the tumor unheated while generating too much heat in the surrounding normal tissues.

In this study, magnetic resonance thermal imaging using the PRFS technique was used to measure 2D temperature rise distributions in four cross sections of large extremity soft tissue sarcomas to allow for real time steering during HT treatments. The goal of this clinical protocol was to quantify the correlation between temperatures measured invasively with temperatures measured non-invasively with MRTI. MR thermometry has been used for measuring power deposition distributions in phantoms with resolution of 0.3–0.5 °C. Clinical studies have also reported resolution of 0.5–1 °C.[11]

The success of the PRFS technique in accurately measuring the changes in temperature in a phantom/living tissue in hyperthermia applications depends on many factors, one of the most important is the interface between the magnet and the hyperthermia applicator used. Other groups have reported their validation studies[28] using a commercially available (in Europe) hyperthermia applicator (Sigma Eye, BSD Corp., 100 MHz) interfaced with a Siemens magnet. At our institution, however, for this group of patients we used an in-house custom applicator with a different antenna configuration (24 cm diameter MAPA, 140 MHz) interfaced with a different magnet (GE Signa Excite). We have established clear differences in the system performance even moving from magnet

TABLE I. Summary of the results for the three example ROIs considered: Viable tumor, necrotic tumor, and fat/tumor interface (normal tissue) based on a Bland–Altman comparison between Luxtron and MR measurements.

	Viable tumor ROI (P14)	Necrotic tumor ROI (P8)	Fat/tumor ROI (P13)
Sample size (time points)	69	60	60
Mean of difference ±95% CI (°C)	0.162 ± 0.121	−0.480 ± 0.152	0.047 ± 0.120
Standard deviation (°C)	0.503	0.590	0.465
Lower limit ±95% CI (°C)	−0.824 ± 0.207	−1.637 ± 0.262	−0.865 ± 0.207
Upper limit ±95% CI (°C)	1.147 ± 0.207	0.676 ± 0.262	0.959 ± 0.207

to magnet (same strength, same manufacturer), so it was imperative to do extensive characterization specific to the new applicator and MR equipment, part of which is summarized in the present manuscript.

Moreover, in the validation study available in literature for sarcomas,[28] temperature-sensitive sequences were acquired "every 10–20 min," whereas in our protocol, we acquired images every minute in each slice to allow for feedback for power steering. This allowed for a more comprehensive validation of the MR thermometry and has significant implications for utility in future monitoring and real time control of heating, demonstrating that MR thermometry can provide a good temporal resolution with good accuracy to allow for steering of the heat. Our present study describes important steps forward toward rapid volumetric real time image guided hyperthermia treatments with temperature accuracy in line with hyperthermia treatment requirements (<1 °C accuracy in 1 min feedback time) rather than slower and/or lower resolution temperature acquisition described previously. With update times of the order of minutes, the real time treatment control claim made here is in agreement with an accepted definition of "real time" given for thermal therapies by Rieke and Pauly,[22] as "an update time that is small compared to significant changes in temperatures during treatment." This update time is different in hyperthermia (minutes or more) versus ablation therapies (less than a second). This whole process lends credibility to the idea that future hyperthermia systems could use image feedback to control and focus heating in tumors.

In the present study, overall agreement was excellent, with mean differences of 0.91 °C for all power on time and 0.85 °C for the steady-state portion of treatment. When just tumor ROIs were analyzed, the mean differences were 0.74 and 0.62 °C, respectively. The reason for improved correlation was almost certainly due to reduced temperature gradients inside the tumor away from tissue interfaces, such that the temperature of a volume averaged ROI is more similar to the temperature of the corresponding fixed point (invasive probe). It was anticipated that this analysis would be challenging since it requires us to compare the temperature of a single point monitored by an invasive sensor with a spatially averaged tissue temperature from a ROI volume that can average pixels with large heterogeneity: Perfused tumor, necrotic tumor, normal tissue. The heterogeneity of tissue composition averaged in a ROI is an important factor in the MR thermometry validation, hence, our decision to report the validation separately for all ROIs, and then for the necrotic/viable tumor and normal ROIs, respectively. Some normal ROIs, like the one exemplified in Fig. 7, were located at tumor/fat interface. In this case, averaging of pixels that contain fat was inevitable. It is well known that the PRFS method works in aqueous tissues. The temperature sensitivity of fat, however, is several orders of magnitude smaller than in aqueous tissue, indicating that the thermometry inside fatty tissue is difficult, leading even to temperature errors.[22] However, it is important to learn and quantify if possible the differences between the invasive and MR thermometry at interfaces, as these are areas of great interest with usually viable (highly perfused) tumor.

It is also known that temperature-induced changes in the electrical conductivity of tissue especially when large volumes of tissue are uniformly heated, as is the case in hyperthermia, can invalidate the scaling of the temperature-induced phase shift with the echo time, TE.[22] This is another reason why validation of MR thermometry has to be done for each heated site and scanner/applicator combination.

Several problems were resolved during the course of this initial ten patient MRTI feasibility trial, which are described in more detail elsewhere.[37] We had mentioned earlier that changes were made to the applicator to allow for drift correction. This has been the first reported use and validation of oil references in a hyperthermia treatment. We have shown in this paper that they work as an efficient correction method for field drift in heated *in vivo* tissue.

Another problem that was addressed was related to limiting the motion induced artifacts by securing the cylindrical MAPA applicator to the MR table and supporting the extremity inside the applicator to minimize movement during treatment. This is important as the accuracy of the temperature rise images is highly dependent on the applicator and/or tissue motion relative to the baseline images taken at the beginning of the hour long treatment. Other investigators[22,38] also noted the sensitivity of the PRFS method to motion and proposed a variety of solutions typically based on rapid imaging, image registration, navigator echoes, or use of unheated tissues to provide temperature reference. Future work will investigate the clinical robustness of such methods, but detailed discussion of these methods is beyond the scope of this work. Another important improvement to the system was filling the water bolus with heavy water (D_2O) rather than de-ionized water. This allowed the bolus to be circulated at a constant temperature without causing flow artifacts and thus improve patient comfort.

V. CONCLUSIONS

Our study demonstrates that for the evaluable HT treatments performed in the integrated 1.5 T MR scanner with RF phased array heating applicator, we achieved excellent correlation of tissue temperature rise ($\Delta T < 1$ °C) as calculated from PRFS-based MRTI regions of interest and compared to nearby invasive probe measurements. With 1 min temporal resolution of measurements in four image planes, this noninvasive MRTI approach has demonstrated its feasibility for accurate monitoring and real time steering of heat into tumors at depth in the body. However, accurate 3D localization of invasive sensors and MR imaging artifacts from motion of the coupling fluid and/or tissue during treatment were serious challenges that limited the number of successful comparisons in the initial cohort of ten patients. Subsequent developments are already proving useful to enhance the reliability of this noninvasive volumetric thermometry approach, including use of gadolinium filled catheter inserts during initial local-

ization scans for more precise probe localization, D_2O as a zero signal coupling fluid, and applicator stabilization mounts to restrict patient movement.

As MRTI technology continues to mature, it offers opportunities for more than just temperature measurement. It can provide volumetric thermal data that can be correlated with volumetric physiological parameters as established with imaging, like perfusion, cell kill, and hypoxia. By monitoring real time changes in temperature during heating, MRTI can provide critical feedback for dynamic control of treatment delivery.

This type of high precision thermometry demonstrated here is a very useful result to the hyperthermia community to support continued development of hyperthermia systems that will rely on monitoring and control noninvasively rather than from a restricted set of implanted sensors.

ACKNOWLEDGMENT

This work was supported by NCI Grant No. CA42745.

[a]Author to whom correspondence should be addressed. Electronic mail: oana.craciunescu@duke.edu; telephone: (919) 660-2192.

[1]B. C. P. O'Sullivan, C. Euler, and C. Catton, "Soft tissue sarcoma," in *Clinical Radiation Oncology*, edited by G. a. Tepper (Churchill Livingstone Elsevier, Philadelphia, PA, 2007), Vol. 1, pp. 1519–1550.

[2]H. D. Suit, H. J. Mankin, W. C. Wood, M. C. Gebhardt, D. C. Harmon, A. Rosenberg, J. E. Tepper, and D. Rosenthal, "Treatment of the patient with stage M0 soft tissue sarcoma," J. Clin. Oncol. **6**, 854–862 (1988).

[3]L. B. Harrison, F. Franzese, J. J. Gaynor, and M. F. Brennan, "Long-term results of a prospective randomized trial of adjuvant brachytherapy in the management of completely resected soft tissue sarcomas of the extremity and superficial trunk," Int. J. Radiat. Oncol., Biol., Phys. **27**, 259–265 (1993).

[4]L. R. Prosnitz, P. Maguire, J. M. Anderson, S. P. Scully, J. M. Harrelson, E. L. Jones, M. Dewhirst, T. V. Samulski, B. E. Powers, G. L. Rosner, R. K. Dodge, L. Layfield, R. Clough, and D. M. Brizel, "The treatment of high-grade soft tissue sarcomas with preoperative thermoradiotherapy," Int. J. Radiat. Oncol., Biol., Phys. **45**, 941–949 (1999).

[5]R. D. Issels, L. H. Lindner, P. Wust, P. Hohenberger, K. Jauch, S. Daugaard, U. Mansmann, W. Hiddemann, J. Blay, and J. Verweij, "Regional hyperthermia (RHT) improves response and survival when combined with systemic chemotherapy in the management of locally advanced, high grade soft tissue sarcomas (STS) of the extremities, the body wall and the abdomen: A phase II randomised pros," J. Clin. Oncol. **25**, 10009 (2007).

[6]J. J. Lagendijk, G. C. Van Rhoon, S. N. Hornsleth, P. Wust, A. C. De Leeuw, C. J. Schneider, J. D. Van Dijk, J. Van Der Zee, R. Van Heek-Romanowski, S. A. Rahman, and C. Gromoll, "ESHO quality assurance guidelines for regional hyperthermia," Int. J. Hyperthermia **14**, 125–133 (1998).

[7]M. W. Dewhirst *et al.*, "RTOG quality assurance guidelines for clinical trials using hyperthermia," Int. J. Radiat. Oncol., Biol., Phys. **18**, 1249–1259 (1990).

[8]B. Emami *et al.*, "RTOG quality assurance guidelines for interstitial hyperthermia," Int. J. Radiat. Oncol., Biol., Phys. **20**, 1117–1124 (1991).

[9]M. D. Sapozink *et al.*, "RTOG quality assurance guidelines for clinical trials using hyperthermia for deep-seated malignancy," Int. J. Radiat. Oncol., Biol., Phys. **20**, 1109–1115 (1991).

[10]P. Wust, C. H. Cho, B. Hildebrandt, and J. Gellermann, "Thermal monitoring: Invasive, minimal-invasive and non-invasive approaches," Int. J. Hyperthermia **22**, 255–262 (2006).

[11]J. Gellermann, M. Weihrauch, C. H. Cho, W. Wlodarczyk, H. Fahling, R. Felix, V. Budach, M. Weiser, J. Nadobny, and P. Wust, "Comparison of MR-thermography and planning calculations in phantoms," Med. Phys. **33**, 3912–3920 (2006).

[12]J. Gellermann, W. Wlodarczyk, H. Ganter, J. Nadobny, H. Fahling, M. Seebass, R. Felix, and P. Wust, "A practical approach to thermography in a hyperthermia/magnetic resonance hybrid system: Validation in a heterogeneous phantom," Int. J. Radiat. Oncol., Biol., Phys. **61**, 267–277 (2005).

[13]E. Hutchinson, M. Dahleh, and K. Hynynen, "The feasibility of MRI feedback control for intracavitary phased array hyperthermia treatments," Int. J. Hyperthermia **14**, 39–56 (1998).

[14]K. S. Cheng, V. Stakhursky, O. I. Craciunescu, P. Stauffer, M. Dewhirst, and S. K. Das, "Fast temperature optimization of multi-source hyperthermia applicators with reduced-order modeling of 'virtual sources'," Phys. Med. Biol. **53**, 1619–1635 (2008).

[15]V. L. Stakhursky, O. Arabe, K. S. Cheng, J. Macfall, P. Maccarini, O. Craciunescu, M. Dewhirst, P. Stauffer, and S. K. Das, "Real-time MRI-guided hyperthermia treatment using a fast adaptive algorithm," Phys. Med. Biol. **54**, 2131–2145 (2009).

[16]H. E. Cline, K. Hynynen, E. Schneider, C. J. Hardy, S. E. Maier, R. D. Watkins, and F. A. Jolesz, "Simultaneous magnetic resonance phase and magnitude temperature maps in muscle," Magn. Reson. Med. **35**, 309–315 (1996).

[17]G. C. van Rhoon and P. Wust, "Introduction: Non-invasive thermometry for thermotherapy," Int. J. Hyperthermia **21**, 489–495 (2005).

[18]B. Denis de Senneville, B. Quesson, and C. T. Moonen, "Magnetic resonance temperature imaging," Int. J. Hyperthermia **21**, 515–531 (2005).

[19]J. Gellermann, W. Wlodarczyk, A. Feussner, H. Fahling, J. Nadobny, B. Hildebrandt, R. Felix, and P. Wust, "Methods and potentials of magnetic resonance imaging for monitoring radiofrequency hyperthermia in a hybrid system," Int. J. Hyperthermia **21**, 497–513 (2005).

[20]K. Kuroda, "Non-invasive MR thermography using the water proton chemical shift," Int. J. Hyperthermia **21**, 547–560 (2005).

[21]N. McDannold, "Quantitative MRI-based temperature mapping based on the proton resonant frequency shift: Review of validation studies," Int. J. Hyperthermia **21**, 533–546 (2005).

[22]V. Rieke and K. B. Pauly, "MR thermometry," J. Magn. Reson Imaging **27**, 376–390 (2008).

[23]J. R. MacFall and B. J. Soher, "From the RSNA refresher courses: MR imaging in hyperthermia," Radiographics **27**, 1809–1818 (2007).

[24]D. L. Carter, J. R. MacFall, S. T. Clegg, X. Wan, D. M. Prescott, H. C. Charles, and T. V. Samulski, "Magnetic resonance thermometry during hyperthermia for human high-grade sarcoma," Int. J. Radiat. Oncol., Biol., Phys. **40**, 815–822 (1998).

[25]O. I. Craciunescu, S. K. Das, R. L. McCauley, J. R. MacFall, and T. V. Samulski, "3D numerical reconstruction of the hyperthermia induced temperature distribution in human sarcomas using DE-MRI measured tissue perfusion: Validation against non-invasive MR temperature measurements," Int. J. Hyperthermia **17**, 221–239 (2001).

[26]O. I. Craciunescu, T. V. Samulski, J. R. MacFall, and S. T. Clegg, "Perturbations in hyperthermia temperature distributions associated with counter-current flow: Numerical simulations and empirical verification," IEEE Trans. Biomed. Eng. **47**, 435–443 (2000).

[27]M. Peller, H. M. Reinl, A. Weigel, M. Meininger, R. D. Issels, and M. Reiser, "T1 relaxation time at 0.2 Tesla for monitoring regional hyperthermia: Feasibility study in muscle and adipose tissue," Magn. Reson. Med. **47**, 1194–1201 (2002).

[28]J. Gellermann, B. Hildebrandt, R. Issels, H. Ganter, W. Wlodarczyk, V. Budach, R. Felix, P. U. Tunn, P. Reichardt, and P. Wust, "Noninvasive magnetic resonance thermography of soft tissue sarcomas during regional hyperthermia: Correlation with response and direct thermometry," Cancer **107**, 1373–1382 (2006).

[29]J. Gellermann, H. Faehling, M. Mielec, C. H. Cho, V. Budach, and P. Wust, "Image artifacts during MRT hybrid hyperthermia—Causes and elimination," Int. J. Hyperthermia **24**, 327–335 (2008).

[30]B. M. Dale, J. A. Jesberger, J. S. Lewin, C. M. Hillenbrand, and J. L. Duerk, "Determining and optimizing the precision of quantitative measurements of perfusion from dynamic contrast enhanced MRI," J. Magn. Reson Imaging **18**, 575–584 (2003).

[31]Y. Zhang, W. T. Joines, R. L. Jirtle, and T. V. Samulski, "Theoretical and measured electric field distributions within an annular phased array: Consideration of source antennas," IEEE Trans. Biomed. Eng. **40**, 780–787 (1993).

[32]Y. Ishihara, A. Calderon, H. Watanabe, K. Okamoto, Y. Suzuki, and K. Kuroda, "A precise and fast temperature mapping using water proton chemical shift," Magn. Reson. Med. **34**, 814–823 (1995).

[33]J. R. MacFall, D. M. Prescott, H. C. Charles, and T. V. Samulski, "1H MRI phase thermometry in vivo in canine brain, muscle, and tumor tissue," Med. Phys. **23**, 1775–1782 (1996).
[34]R. Franke, "Smooth interpolation of scattered data by local thin plate splines," Comput. Math. Appl. **8**, 273–281 (1982).
[35]C. Wyatt, B. Soher, V. Stakhursky, P. Maccarini, C. Charles, P. Stauffer, and J. MacFall, "Hyperthermia MRI temperature measurement: Evaluation of measurement stabilization strategies for extremity and breast tumors," Int. J. Hyperthermia **25**(6), 422–433 (2009).
[36]J. M. Bland and D. G. Altman, "Statistical methods for assessing agreement between two methods of clinical measurement," Lancet **1**, 307–310 (1986).
[37]P. Stauffer, O. Craciunescu, P. Maccarini, C. Wyatt, K. Arunachalam, O. Arabe, V. Stakhursky, Z. Li, B. Soher, J. MacFall, S. Rangarao, K. S. Cheng, S. Das, M. W. Dewhirst, T. Wong, E. Jones, and Z. Vujaskovic, "Clinical utility of magnetic resonance thermal imaging (MRTI) for real time guidance of deep hyperthermia," Proc. SPIE **7181**, 718101-1–718101-12 (2009).
[38]B. D. de Senneville, C. Mougenot, and C. T. Moonen, "Real-time adaptive methods for treatment of mobile organs by MRI-controlled high-intensity focused ultrasound," Magn. Reson. Med. **57**, 319–330 (2007).